International Journal of
INTELLIGENT SYSTEMS AND APPLICATIONS IN ENGINEERING
ISSN:2147-6799 www.ijisae.org Original Research Paper

Enhanced Open-Circuit Fault Detection and Localization in Electric Vehicle Inverter Switches using Hybrid SGO-FAT Technique

Selvakumar P[1*], Dr. Muthukumaran G[2]

Submitted: 29/01/2024 **Revised**: 07/03/2024 **Accepted**: 15/03/2024

Abstract: This paper proposes a hybrid method for locating and identifying open-circuit problems in electric vehicle inverter switches. The proposed hybrid method is the combined execution of both the Shell Game Optimization and Feedback Artificial Tree technique, and it is commonly named as SGO-FAT technique. The proposed strategy is to provide accurate information on fault location while enhancing the resilience and speed of fault detection. The SGO technique is employed to identify system defects under steady and transient state condition of speed drive. The Feedback Artificial Tree (FAT) methodology is integrated to enhance fault localization accuracy. The proposed SGO-FAT method is to enhance the effectiveness of localizing and detecting open-circuit faults with EVs' inverter switches. The proposed technique is implemented on the MATLAB platform, and compared with current methods. The results show that the better proposed approach is at accuracy and stability, characterized by the lowest error values ISE: 5.341, ITAE: 0.3035, IAE: 0.00779 than other existing techniques, like Heap-based optimizer (HBO), Ant Colony Optimization (ACO) algorithm and Salp Swarm Algorithm (SSA).

Keywords**:** *Fault Detection, Active Three-Phase Neutral-Point-Clamped Inverter, Single Localization, Shell Game Optimization, Battery or Inverter Switch Faults, Feedback Artificial Tree.*

1. Introduction

Two-level inverter topologies are extensively used in the realm of vehicle traction applications because of their maturity [1]. With these, the powertrain loses vehicle controllability and may have to stall rather than providing redundancy in the event of a problem [2]. To address this issue, redundant two-level inverter topologies have been suggested [3, 4]. These include paralleling extra inverter legs or switches and implementing complex circuitry for short-circuit protection. Conversely, multilevel inverter topologies may provide redundancy along with further advantages like reduced common mode voltage, improved power density, or lessened switch stress [5].

As electric vehicles (EVs) become increasingly integral to modern transportation, the reliability and performance of their powertrain components are paramount [6]. Among these components, the inverter serves a critical role in converting DC from the battery vehicle into AC for the electric motor [7].However, the emergence of open-circuit faults in inverter switches presents important to the seamless operation of EVs [8]. Open-circuit faults refer to disruptions in the electrical connectivity within the inverter switches, creating gaps in the circuit and impeding the flow of current [9]. These faults can stem from various factors, such as component aging, manufacturing defects, or external stressors, and their occurrence can lead to a range of operational issues [10].

Maintaining the safety, effectiveness, and lifetime of the electric vehicle powertrain requires prompt identification and accurate localization of open-circuit defects [11]. Open-circuit faults in inverter switches can lead to disruptions in the power flow, compromising the efficiency and overall functionality of the EV powertrain [12]. Timely and accurate detection of these faults is crucial for preventing potential hazards, ensuring passenger safety, and minimizing downtime for maintenance [13]. Furthermore, localizing the specific points of failure within the inverter switches is essential for effective and targeted repairs [14].

1.1. Objectives and Contribution:

- The key contribution of this manuscript is to propose a hybrid Shell Game Optimization-Feedback Artificial Tree (SGO-FAT) method for detecting single battery or inverter switch faults through a connected neutral point during the operation of a common, active 3-phase neutral-point-clamped (NPC) inverter.
- Utilizes Shell Game Optimization (SGO) for fault detection under various operational conditions, showcasing adaptability in both steady-state and transient states.

[1]Research Scholar, Department of Electrical and Electronics Engineering, Hindustan Institute of Technology and Science, Chennai, Tamil Nadu, India.*
[1]ORCID ID: https://orcid.org/0009-0003-4620-9176*
[2]Professor, Department of Electrical and Electronics Engineering, Hindustan Institute of Technology and Science, Chennai, Tamil Nadu, India
[2]Email: gmkumaran@hindustanuniv.ac.in
** Corresponding Author Email: cpselva.kumar@gmail.com*

- The novelty of this manuscript proposes a hybrid technique for highly effective open-circuit fault detection and localization in EV inverters.
- Enables swift direct action following fault detection, contributing to the overall resilience of the EV inverter system.
- Comparative analysis against existing techniques demonstrates the superior performance of the SGO-FAT method, affirming its efficacy in electric vehicle applications.
- The remainder of the paper is as follows: Section 2 reviews literature survey, section 2.1 shows the background. Section 3 defines the structure of common, active 3-Phase NPC inverter with NP connection. Section 4 defines the investigation of single battery failures and the controls of drive-train. Section 5 describes the proposed approach based online open-circuit. Section 6 illustrates results and discussion. Section 7 concludes the paper.

2. Recent Research Works: A Brief Review

Numerous studies were already published in the literatures on basic of fault detection, localization for EVs utilizing several methods as well as features. Certain of them are reviewed here.

An intelligent method was presented by Selvakumar and Muthukumaran [15] to locate and identify a phase fault or inverter switch failure in a 3 Level-Active Neutral Point Clamped Inverter. Furthermore, a 3L-ANPC inverter has the capacity to recover control over an EV's power train and prevent stalling even in the event of a malfunction. Therefore, an efficient fault diagnostic technique was required in order to determine the kind of phase defect by using a support vector machine, a machine learning model built from labels for training data sets with tasks for regression and classification. Ultimately, a Deep Neural Network, which has layers of neurons between the input and output layers and more precisely incorporates the feature extraction process, can be used to locate a failed switch. To demonstrate the outstanding reliability of the open winding interior permanent magnet synchronous motor drive system provided by twin inverters over the whole EV speed range.

Matsumori et al. [16] have introduced innovative fail-safe action plan and fault detection algorithms for inverter power devices. The microcomputer processed the measured three-phase fault currents analytically and logically to produce the novel algorithms for the inverter power device fault detection. The fail-safe action approach was created to reduce traction motor vibration that results from an unintentional torque ripple when an inverter device fault condition occurs. This was accomplished by quickly balancing the three-phase fault currents with a single inverter, utilizing two inverters to balance the three-phase imbalanced fault currents.

Kumar [17] presented a fast multiple open circuit fault detection and defective switch localization system using a single switch fault-tolerant cascaded H-bridge multilevel inverter with level-shifted pulse width modulation. A straightforward redundant power cell configuration allows the multilayer inverter to be fault-tolerant. The OCF for the special and quick switch fault localization and tolerance algorithm has a healthy anti-parallel diode. With CHB-MLI, upper or lower switches can bypass the OCF Bridge without the requirement for an extra semiconductor device. As a result, it was necessary to precisely localize switch faults inside the H-bridge.

Reyes-Malanche et al. [18] confirmed a unique low-cost computing method that directly analyzes the electric phase currents from a power inverter in the time domain and finds open-circuits by using three rotatory reference systems and simple arithmetic operations. The offered method allows for the precise identification of both the broken switch and the specific power supply phase.

Jiang et al. [19] presented a technique for locating open-circuit issues in permanent magnet synchronous motors powered by two inverters and a single dc source that had open ends. The driving systems' speed range and tolerance capacity could be improved by the OEW-PMSM. However, the symmetry of the twin inverter architecture makes it impossible for open-circuit fault detection techniques for Y-connected PMSMs to locate the problematic switch. The method's first stage involved identifying incorrect switch combinations using the error between the normalized average value and the average value of the zero-sequence reference voltage. The next step was to use a specific fault combination to identify the faulty switch.

Rtibi et al. [20] verified the five-level NPC inverter in an electric car system employing the ant colony optimization technique. Two induction motors, each driven by a single NPC inverter, made up the system that was demonstrated. The front and rear axles, respectively, were equipped with the two IMs. The three-phase, five-level NPC inverter's rotor-flux-oriented control was achieved through the use of Phase Disposition Carrier-PWM techniques. The examination of total harmonic distortion (THD%) was very interesting. However, the suggested ACO method correctly calculated the dynamic loading conditions of an EV driven by an IM, the necessary PI parameter to determine the optimal PI regulator gains settings.

Ahmad et al. [21] presented a unique approach to defect localization and detection. The suggested approach identified and localized defects using a harmonic component depending on switching frequency. After the

problem was identified, a post-fault restoration and control technique was used to minimize input current ripple in the photovoltaic panel and to guarantee equitable current sharing amongst the remaining functional modules while staying within their maximum current rating.

2.1. Background of the Research Work

Recent studies expose that it is essential to locate and identify open-circuit defects in inverter switches. The literature has various fault detection, localization approaches to common NPC converters, often utilized on grid-connected applications, such as rectifiers or inverters. HBO performance can be sensitive to parameter settings, and finding the optimal configuration may pose a challenge. Inappropriate parameter choices could lead to suboptimal results or hinder convergence. ACO performance is influenced by various parameters, such as pheromone evaporation rate and exploration factor. Tuning these parameters for different applications and fault scenarios can be non-trivial and time-consuming. Salp Swarm Algorithm (SSA) faces challenges in ensuring effective global exploration of the solution space. The algorithm must efficiently explore diverse regions to discover optimal solutions, particularly in complex fault detection scenarios. Similar to other optimization methods, SSA is sensitive to parameter settings, posing a challenge in identifying suitable values for different applications and systems. To overcome these challenges, optimum detection utilized advanced technology is required. The above mentioned disadvantages are inspired to do this work.

3. Configuration of Common, Active Three-Phase NPC Inverter with NP Connection

One of multilevel power inverter is the NPC inverters which are characterized by a use of clamping diodes [22] to ensure a suitable voltage distribution across a power switches. Fig 1 reveals the circuit diagrams of (a) NPC inverter, (b) ANPC with NP connection. This paper utilized the common NPC, and ANPC with MOSFETs with NP linking. SVM is a general approach utilized to operate as well as produce an appropriate output voltage in a 3-level NPC multilevel inverter [23].

$$V_{X-np}^{*} = \frac{V_{dc}}{2} S_X^{*} \tag{1}$$

here V_{X-np}^{*} is denoted *as* phase voltage X using $\{A,B,C\} \in X$, switching state is denoted as S_X^{*}. In a specific time interval, the mean of switching combinations is provides the appropriate output voltage. The line voltage with maximum RMS value is described as,

$$V_{ll,rms}^{*} = \frac{V_{dc1}+V_{dc2}}{\sqrt{2}} = 0.707 V_{dc} \tag{2}$$

Thus, when the supply of a voltage source is turned off, half of the maximum output voltage is lowered. When the NPC inverter operates through SVM, and then the dc side current spectrum is recognized. NP current is also known as the third harmonic current component that runs in positive, negative NPC inverter DC-link. Then, the linking of NP is based on the capacitor closing and inverter midpoint connection.

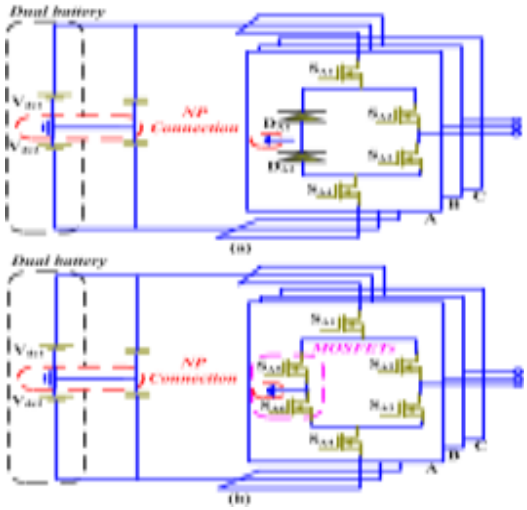

Fig 1: Circuit diagram of (a) NPC inverter, and (b) ANPC with NP connection

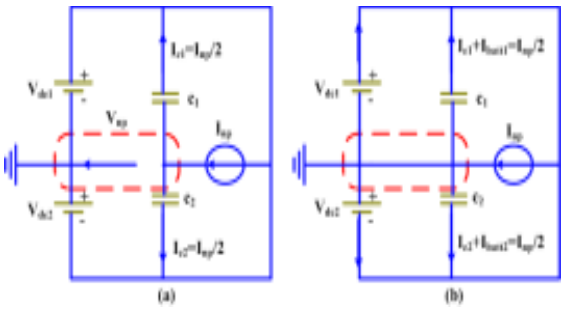

Fig 2: The propagation path of 3rd harmonic current in (a) Oscillation of capacitor voltage, (b) NP connection

Fig 2 illustrates the propagation path of the 3rd harmonic current in (a) Oscillation of capacitor voltage and (b) Neutral Point connection. In the oscillation of capacitor voltage, it is observed that the capacitor voltage oscillates at a frequency that is three times greater than the voltage output. The SVM approach is then employed to lessen the 3rd harmonic-current based on losses in the battery, motor, and inverter. The NP connection's capacity to maintain powertrain running in the event of a single switch or battery failure is a crucial benefit, commonly known as the "limp-home" model. This feature enhances the reliability and resilience of the powertrain system.

4. Analysis of Single Inverter or Single Battery Faults and the Controls of the Drive Train

The open circuit switch faults detection is more concentrated in this paper [24]. Fig 3 depicts the cascaded control system of the drivetrain. The drivetrain comprises a speed controller, a current controller, and a load. The first order closed loop transfer function is described as,

$$G_{Clos}(S) = \frac{\beta}{S+\beta} = \frac{H(S)G(S)}{1+H(S)G(S)} \tag{3}$$

here bandwidth is denoted as β .

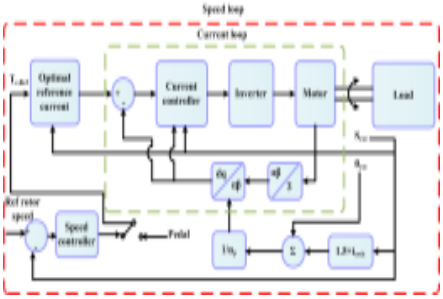

Fig 3: Drive train in cascaded control

The active damping is presented in the transfer function, so it is rewritten as,

$$G^{*}_{Clos}(S) = \frac{1}{L_{Sq}S + r_S + r_{Aq}} \tag{4}$$

here stator resistance is denoted as r_S , active damping in quadrature-axis is denoted as r_{Aq} . PI controller is utilized to control the current. So the transfer function with quadrature current controller is described as,

$$G^{*}_{ClosCq}(S) = \frac{I_{sq}}{I_{Sq\,\mathrm{Re}\,f}} = \frac{\beta_C}{S+\beta_C} = \frac{H_{Cq}(S)G^{*}_{Cq}(S)}{1+H_{Cq}(S)G^{*}_{Cq}(S)} \tag{5}$$

hence the parameter of the current controller at quadrature axis is described as,

$$H^{*}_{Cq}(S) = \beta_C L_{Sq} + \frac{\beta_C(r_S + r_{Aq})}{S} = K_{pq} + \frac{K_{iq}}{S} \tag{6}$$

Using the damping function, the transfer function is described as,

$$G^{*}_{Cq}(S) = g\frac{\beta_C}{S+\beta_C} = \frac{1}{L_{Sq}S + r_S + r_{Aq}} \tag{7}$$

The active damping coefficient at quadrature axis is described as,

$$r_{Aq} = \beta_C L_{Sq} - r_S \tag{8}$$

5. Proposed Approach Based Online Open-Circuit Diagnosis

The proposed method's objective is to locate and diagnose open-circuit problems. The control system of this approach is illustrated in Fig 4. The faulty half leg must be identified in order to determine the open-circuit problem that arises when operating online [25]. For a half-leg operation, the SVM pattern undergoes a two-level process using a single battery. The average Park vector approach is then employed to identify the defective half leg, relying on a Clark transformation of average phase current values, which produces a non-zero value at the fault position.

Fig 4: Control structure of the proposed approach

To precisely regulate a switch fault on the identified half leg, a transformation is utilized. The fault detection process begins with normal operation data, which is then subjected to the SGO-based fault detection. Once a fault is detected using SGO, the next step involves localization through the proposed FAT approach. The next section goes into further detail on the FAT and SGO process step-by-step.

5.1. SGO for Optimal Fault Detection

Shell Game Optimization significantly contributes to the enhanced open-circuit fault localization and detection in electric vehicle inverter switches through its optimization capabilities. Inspired by the strategic dynamics of the shell game, SGO excels in optimizing decision-making processes within the fault detection system. By dynamically adjusting parameters and thresholds, SGO ensures that the system is finely tuned for optimal performance, leading to increased accuracy in identifying open-circuit faults. Its adaptive nature allows it to explore complex solution spaces, making it particularly effective in diverse operating conditions. Overall, SGO brings a strategic and adaptive optimization approach that improves the reliability of the fault detection system [26]. The step by step process is given below,

Step 1: Initialization

The voltage and current is initialized, so the input vector is calculated below,

$$X_i = [(V_1, I_1, P_1)^1, (V_2, I_2, P_2)^2 \ldots (V_n, I_n, P_n)^n] \quad (9)$$

Step 2: Random formation

Create an approximate input variable using the eqn as below,

$$x_i = \left(y_i^1 \ldots., \; y_i^d \ldots., \; y_i^n \right) \quad (10)$$

where the random variable of fault event x_i is depending on the fitness function value that was achieved.

Step 3: Evaluation of Fitness

Here, equation (11) is used to evaluate the fitness function as below, which is an objective activity.

$$Obj = \min\{E\} \quad (11)$$

here the estimated and measurement currents are used to determine the goal function, which is error minimization.

Step 4: Calculation of Phase Charge

The phase charge is calculated based on the park and Clarke transform.

Step 5: Selecting three shells

Based on the phase charge, 3 shells are set like 1 is better; another 2 are chosen at random.

$$Operator = \begin{cases} H_1 = ball = X_{bst} \\ H_2 = X_{r1} \\ H_3 = X_{r2} \end{cases} \quad (12)$$

The best value is given to the half leg and the other values are given to the battery operation. It checks the fault condition and given to inner and outer switch.

Step 6: Determine accuracy and intelligence

The objective is examined for each function and the accuracy is determined using this condition,

$$A_i = \frac{f_{it(i)} - f_{it}(X_{worst})}{\sum_{l=1}^{n} \left[f_{it(l)} - f_{it}(X_{worst}) \right]} \quad (13)$$

Step 7: Simulating the state of guess

The vector equation is employed to assess each X_{worst} fitness results, minimizing and maximizing as follows:

$$G(x) = \begin{cases} s_1 = If \; A_i > G_1 \\ s_2 = If \; A_i > G_2 \\ s_3 = else \end{cases} \quad (14)$$

where right deduction to 1st and 2nd choice is denoted as G_1, G_2.

Step 8: Updation

Update values of values utilizing the eqn as follows,

$$Y_i^D = Y_i^D + dY_{i,b}^D + dY_{i,S_2}^D + dY_{i,S_3}^D \quad (15)$$

where the updated value is denoted as $dY_{i,b}^D, dY_{i,S_2}^D, dY_{i,S_3}^D$

If all of the parameters have been modified, proceed to the next step or return to step 6.

Step 9: Termination

When the criterion for termination meets the requirement, obtain the optimal solution, else go to step 2.

5.2. Feedback Artificial Tree algorithm (FAT) for Fault Localization

The Feedback Artificial Tree (FAT) technique contributes significantly to the enhancement of open-circuit localization and detection faults in electric vehicle inverter switches by introducing a structured feedback mechanism. The artificial tree structure facilitates systematic information flow within the fault detection system, providing adaptability and learning capabilities [27]. The step by step procedure of FAT are given below,

Step 1: Initialization

Initialize the branch's input parameters to their initial values, think of a training package, extract the features from the training package equation that is presumptively as follows,

$$T_{st} = \left\{ \left(A_1, B_1 \right), \left(A_2, B_2 \right) \ldots \left(A_n, B_n \right) \right\} \quad (16)$$

Consider, there are multiple branches on the tree.

$$N = \left\{ B_1, B_2, B_3 \ldots B_n \right\} \quad (17)$$

Step 2: Random Process

If the feedback process is started, the input is chosen at random. It is described by,

$$X_N = r(X, R) \quad (18)$$

here ratio of newly chosen branches to the population of branch as R, branch population as X; and chosen population of branch as X_N;

Step 3: Self-propagating operator

If branch territory exceeds congested tolerance, the branch is updated by the self-propagating operator. As a result, the defect value appears below.

$$X_N = X_i + (r(0,1) \times X_{bst} - r(0,1) \times X_i) \times g \quad (19)$$

where constant (g) is used to increase system efficiency and is based on the notion of the golden section.

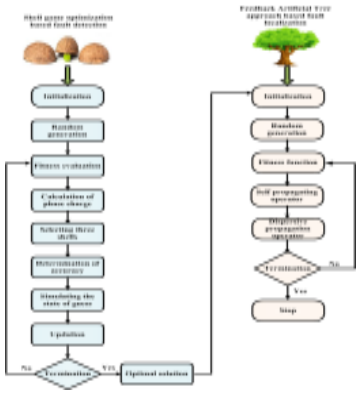

Fig 5: Flowchart of SGO-FAT approach

Step 4: Dispersive propagation operator

The feedback approach uses the dispersive propagation operator to determine the fault site in the event that the branch territory $\geq$exceeds the tolerance for congestion. Next, the location of the fault switch is stated in the following equation:

$$y_{oj} = y_{ij} + r(-1,1) \times (V_i/2) \times a \quad (20)$$

$$y_{tj} = y_{ij} - r(0,1) \times y_{oj} \quad (21)$$

where, $j = 0,1,2...m$, the element of updated branch (X_o, X_t) is y_{oj} , y_{tj} . Flowchart of SGO-FAT approach is shown in Fig 5.

6. Results and Discussion

The simulation outcomes of the proposed methods are shown in this section, with an emphasis on the use of the SGO-FAT methodology for defect localization and detection. The MATLAB platform is used to run the simulations. The proposed approach's performance assessment centers on various phase faults, namely A, AB, ABC, and ABC switch faults. Additionally, the torque characteristics of the motor are analyzed under these fault conditions. Through these simulations, the proposed method's robustness and effectiveness in detecting, localizing, and responding to different fault scenarios are assessed.

Case 1: Analysis of Phase A Fault

Here, the effectiveness of the proposed approach under fault phases. Fig 6 shows the analysis under fault on phase A (a) voltage, and (b) current. Fig 6 (a) displays a voltage analysis under phase A faults. Then, the voltage is normally oscillating among the $-0.8\times10^{-4}$to 0.8×10^{-4} V. The fault is occurring at the time period of 0.42 sec. The same procedure is utilized in the current fault detection. Fig6 (b) displays the current analysis of fault on phase A. The current is oscillating among the $-0.75\times10^{-3}$to 0.75×10^{-3} A. The battery voltage is 100 V at 0 sec, and then it reduced to 99.97 V at the time period of 0.1 sec. Fig 7 presents a detailed analysis of battery performance under a fault on phase A, examining voltage, current, and power characteristics. In Fig 7(a), the battery voltage analysis shows an initial value of 1050 A at 0 sec, swiftly decreasing to 10 A by 0.1 sec, and then gradually approaching zero, reaching a minimum of 0.1 sec. Subplot 7(b) illustrates the battery current, starting at 1050 A and decreasing to 10 A within the first 0.1 sec, followed by near-zero current between 0.2 and 1 sec. In Subplot 7(c), the battery power analysis indicates an initial zero power, followed by a rapid increase to 540 W at 0.1 sec, maintaining a constant value until 1 sec. This detailed depiction provides insights into the battery's voltage, current, and power behaviors during a fault on phase A, facilitating a comprehensive understanding of its responses under these specific conditions.

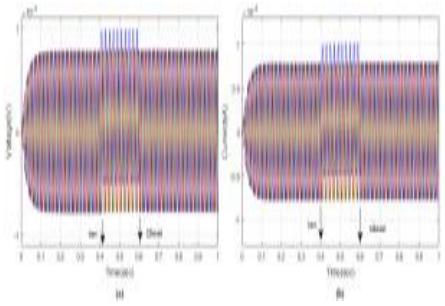

Fig 6: Analysis under fault on phase A (a) voltage, and (b) current

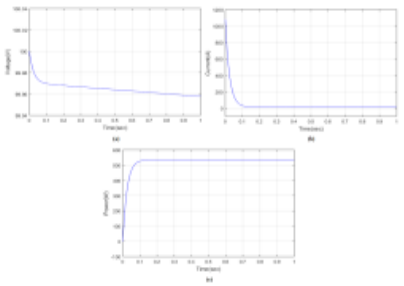

Fig 7: Analysis of battery (a) voltage (b) current, and (c) power under fault on phase A

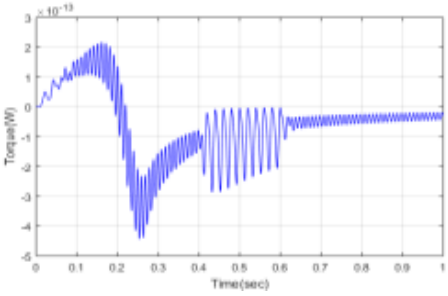

Fig 8: Analysis of torque under fault on phase A

Fig 8 shows the analysis of torque under fault on phase A. The torque is increasing from 0 to 2.1×10^{-13}Nm. After the detection and localization of fault, it oscillation is less

and its value is -0.5×10^{-13} to -0.7×10^{-13} Nm, it is continue up to the period of 1 sec.

Case 2: Analysis of Phase AB fault

This section describes the proposed method performance in the event of a phase AB fault. Fig 9 shows the analysis of fault on phase AB voltage and current. Fig 9 (a) depicts the voltage analysis under phase AB fault. The voltage is normally oscillating among the -0.8×10^{-4} to 0.8×10^{-4} V. The same procedure is utilized in the current fault detection. Fig 9 (b) shows the current analysis of fault on phase AB. The current is oscillating among the -0.75×10^{-3} to 0.75×10^{-3} A. The two level operations is start at 0.6 sec. Then the fault is localized and the current is oscillating again- 0.75×10^{-3} to 0.75×10^{-3} A.

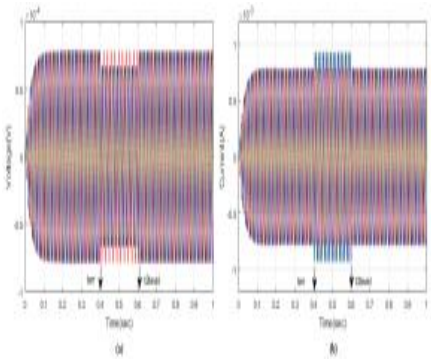

Fig 9: Analysis under fault on phase AB (a) voltage, and (b) current

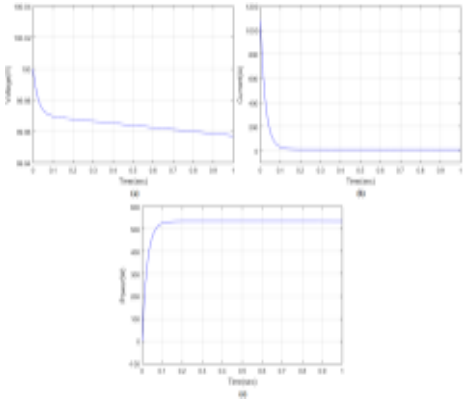

Fig 10: Analysis of battery (a) voltage (b) current, and (c) power under fault on phase AB

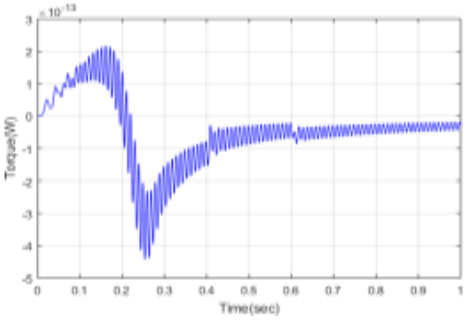

Fig 11: Analysis of torque under fault on phase AB

Fig 10 provides a comprehensive analysis of the battery under a fault on phase AB, examining voltage, current, and power dynamics. In Fig 10(a), the battery voltage initiates at 99.998 V at 0 sec, decreases to 99.97 V by 0.1 sec, and gradually reduces further, reaching 99.958 V at 1 sec. Subplot 10(b) illustrates the battery current, starting at 1050 A at 0 sec, swiftly decreasing to 10 A by 0.1 sec, and maintaining near-zero levels between 0.2 and 1 sec. In Fig 10(c), the battery power is initially zero, then surges to 540 W at 0.1 sec, maintaining a constant value until 1 sec. This detailed analysis provides insights into the battery's voltage, current, and power characteristics during a fault on phase AB, offering a comprehensive understanding of its behavior in such scenarios. Fig 11 shows the analysis of torque under fault on phase AB. The torque is increasing from 0 to 2.1×10^{-13} Nm. After that, the torque oscillation is decreasing to -4.3×10^{-13} Nm. Then the torque oscillation is increasing from -4.3×10^{-13} to -0.7×10^{-13} Nm.

Case 3: Analysis of Phase ABC Fault

This section describes the performance evaluation of the proposed method in the case of an ABC phase fault. Fig 12 provides an analysis of the fault, showcasing the voltage and current in response to the fault on phase ABC.

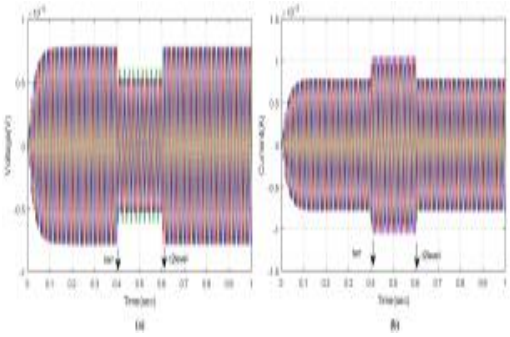

Fig 12: Analysis under fault on phase ABC (a) voltage, and (b) Current

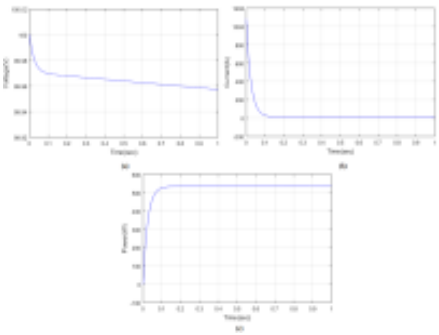

Fig 13: Analysis of battery (a) voltage (b) current, and (c) power under fault on phase ABC

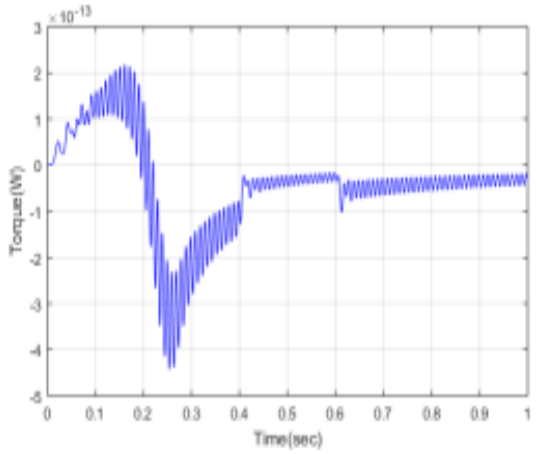

Fig 14: Analysis of torque under fault on phase ABC

Subplot 12 (a) shows the voltage analysis under phase ABC fault. The voltage is normally oscillating among the -0.8×10^{-4} to 0.8×10^{-4} V. The same procedure is utilized in the current fault detection. Fig 12 (b) depicts the current analysis of fault on phase ABC. The current is oscillating among the -0.75×10^{-3} to 0.75×10^{-3} A. Then the fault is localized and the current is oscillating again -0.75×10^{-3} to 0.75×10^{-3} A. Fig 13 presents a comprehensive analysis of the battery under a fault on phase ABC, encompassing voltage, current, and power characteristics. Subplot 13(a) illustrates the battery voltage, starting at 100 V at 0 sec and gradually decreasing to 99.97 V by 0.1 sec, reaching 99.958 V at 1 sec. Subplot 13(b) depicts the battery current, which remains around 0 between 0.2 and 1 sec. Subplot 13(c) focuses on battery power, initially at zero, then increasing to 540 W at 0.1 sec and maintaining a constant value until 1 sec. Fig 14 delves into the torque analysis under the fault on phase ABC, revealing oscillations with minimal variation at 0.4 and 0.6 sec. Following fault localization, torque oscillation diminishes, with variations falling below 0 Nm. This detailed examination provides insights into the battery's voltage, current, power, and torque responses during a phase ABC fault in the system.

Case 4: Analysis of 3 Phase Switch Fault

This section describes the proposed system performs when there are three-phase switch problems, with Fig 15 providing an analysis of the fault on phase ABC, specifically focusing on voltage and current characteristics. In Fig 15(a), the voltage analysis under the phase ABC switch fault is illustrated. The visual representation in this subplot elucidates the system's response and behavior concerning voltage during the occurrence of the three-phase switch fault on phase ABC. The phase ABC voltage is varying from -0.5×10^{-4} V to 1×10^{-4} V. The same procedure is utilized in the current fault detection. Fig 15 (b) shows the current analysis of the switch fault on phase ABC. The current fluctuates between -0.75×10^{-3} A to -787 0.75×10^{-3}. Then the fault is localized and the current is oscillating again -0.75×10^{-3} to 0.75×10^{-3} A.

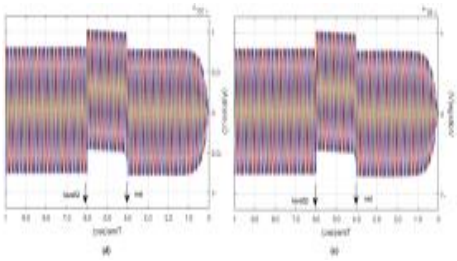

Fig 15: Analysis under switch fault on phase ABC (a) voltage, and (b) current

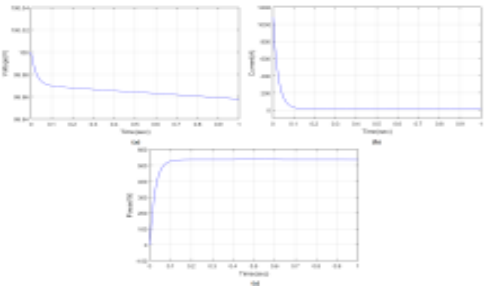

Fig 16: Analysis of battery (a) voltage, (b) current, and (c) power under switch fault on phaseABC

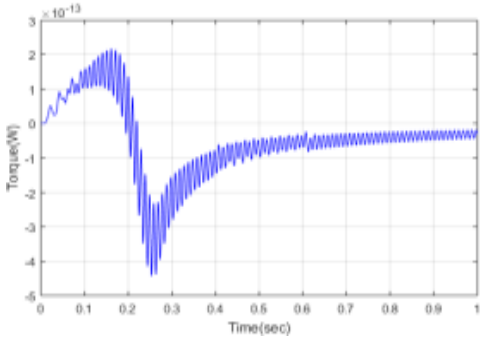

Fig 17: Analysis of torque under switch fault on phase ABC

Fig 16 provides a detailed analysis of battery under a switch fault on phase ABC, covering voltage, current, and power aspects. In Fig 16(a), the battery voltage exhibits a gradual decline, reaching 99.958 V at 1 sec after the onset of the switch fault. Fig 16(b) illustrates the battery current, showing values around 0 during the time period from 0.2 to 1 sec after the fault occurrence. Fig 16(c) focuses on battery power, revealing torque oscillation with minimal variation between 0.4 and 0.6 sec. Subsequent to fault localization, the torque oscillation diminishes, with variations falling below 0 Nm. Fig 17 further explores the torque analysis under the switch fault on phase ABC, providing a comprehensive overview of the battery's voltage, current, and power dynamics in response to the fault condition.

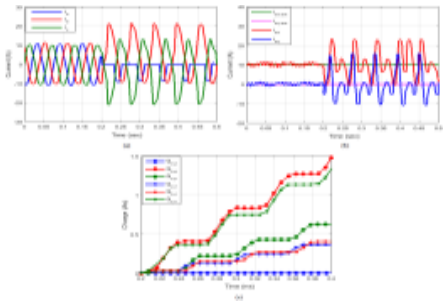

Fig 18: Open-circuit fault detection at S_{a1} for the NPC inverter (a) phase current, (b) fault detection, and (c) phase charges

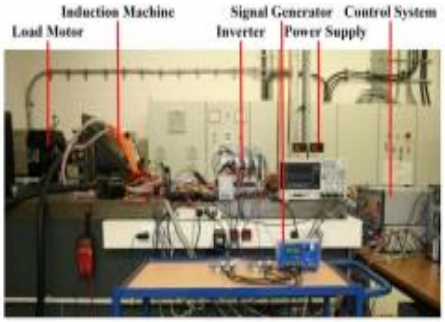

Fig 19: Experimental setup for open-circuit fault test

In Fig 18, the open-circuit fault detection at Sa1 for the NPC inverter is detailed across three facets. Firstly, Fig 18(a) portrays the phase current scenario, where the machine, operating without a load, exhibits amplitude-invariant stator current in the direct axis, aligning with the peak value of the three-phase currents with a 17 Hz fundamental frequency. Secondly, Fig 18(b) focuses on fault detection, specifically identifying a problem in the open circuit at phase A's positive half leg, signaled by the observation of minimum charge for positive phase charge. Lastly, Fig 18(c) delves into phase charges, demonstrating how the minimum positive phase charge serves as an indicator for a phase A positive half leg open-circuit fault. This comprehensive depiction aids in understanding the nuanced aspects of detection of open-circuit faults in the NPC inverter system. The theoretical assumptions and simulation outcomes described above are verified by using a test bench to conduct a basic open-circuit fault test technique, as illustrated in Fig 19.

Table 1: Analysis of voltage and current variation under fault condition

Fault	**Fault duration (Sec)**	**General Voltage**	**Voltage variation (V) at fault**	**Current in normal (A)**	**Current variation (A) at fault**
Phase A, B, C	0.4 to 0.6	- 0.8×10^{-4} to 0.8×10^{-4} V	- 0.5×10^{-4} V to 0.8×10^{-4} V	- 0.75×10^{-3} to 0.75×10^{-3} A	- 0.5×10^{-3} to 0.75×10^{-3} A
Phase AB, BC	0.4 to 0.6	- 0.8×10^{-4} to 0.8×10^{-4} V	- 0.6×10^{-4} V to 0.6×10^{-4} V	- 0.75×10^{-3} to 0.75×10^{-3} A	- 0.9×10^{-3} to 0.9×10^{-3} A
Phase AC, ABC	0.4 to 0.6	- 0.8×10^{-4} to 0.8×10^{-4} V	- 0.51×10^{-4} V to 0.51×10^{-4} V	- 0.75×10^{-3} to 0.75×10^{-3} A	- 1.1×10^{-3} to 1.1×10^{-3} A
Phase ABC switch fault	0.4 to 0.6	- 0.8×10^{-4} to 0.8×10^{-4} V	- 0.5×10^{-4} V to 1×10^{-4} V	- 0.75×10^{-3} to 0.75×10^{-3} A	- 0.5×10^{-3} to 1.01×10^{-3} A

Table 2: Comparison of error values with proposed and existing methods

Solution techniques	**Speed output errors**		
	ISE	**ITAE**	**IAE**
HBO	11.99	0.6701	0.05719
ACO	11.62	0.5901	0.01148
SSA	10.47	0.4892	0.02133
proposed	5.341	0.3035	0.00779

Table 1 is tabulated the analysis of voltage and current variation under fault condition. The phase A, B, C fault, the voltage variation is -0.5×10^{-4}V to 1×10^{-4}V and the current variation become -0.5×10^{-3} to 1×10^{-3} A. The phase AB, BC fault, the voltage variation is -0.6×10^{-4}V to 0.6×10^{-4}V and the current variation become -0.9×10^{-3} to 0.9×10^{-3} A. The phase AC, ABC fault, the voltage variation is -0.51×10^{-4}V to 0.51×10^{-4}V and the current variation become -1.1×10^{-3} to 1.1×10^{-3}A. The phase ABC switch fault, the voltage variation is -0.5×10^{-4}V to 1×10^{-4} V and the current variation become -0.5×10^{-3} to 1.01×10^{-3} A. Table 2 illustrates the comparison of error values with proposed and existing methods. In HBO method, ISE is 11.99; ITAE is 0.6701; and IAE is 0.05719. In ACO mthod, ISE is 11.62; ITAE is 0.5901; and IAE is 0.01148. In SSA method, ISE is 10.47; ITAE is 0.4892; and IAE is 0.02133. The proposed method is the most accurate and stable solution, with the lowest error values ISE (5.341),

ITAE (0.3035), and IAE (0.00779), significantly outperforming HBO, ACO, and SSA. It also maintains the lowest speed output errors.

7. Conclusion

This section concludes the hybrid SGO-FAT method for detecting single battery or inverter switch faults through a linked neutral point during the operation of a common, active 3-phase NPC inverter. Then, the proposed approaches provide proper detection and localization and agree to continue the process directly after the fault. The MATLAB platform is used to implement the proposed method performance. The proposed approach's performance is examined in a number of fault scenarios, including Phase A, AB, ABC faults, and ABC switch faults. The outcomes show that the better the proposed approach is at accuracy and stability, characterized by the lowest error values ISE: 5.341, ITAE: 0.3035, IAE: 0.00779. The application of Hybrid SGO and FAT not only outperforms HBO, ACO, and SSA but also ensures the lowest speed output errors. This research provides a reliable and effective approach for locating and detecting open-circuit problems with electric vehicle inverter switches, advancing the techniques for fault diagnosis in electric vehicle systems.

References

[1] I. Abari, A. Lahouar, M. Hamouda, J. B. Slama and K. Al-Haddad, 2017. Fault detection methods for three-level NPC inverter based on DC-bus electromagnetic signatures. *IEEE Transactions on Industrial Electronics*, 65(7), pp.5224-36.

[2] T. Logeswaran, M. S. Raja, J. B. Hameed and M. Abdulrahim, 2022. Power flow management of hybrid system in smart grid requirements using ITSA-MOAT approach. *AppliedEnergy*, 319, p.119228.

[3] S. Mukherjee, S.K. Giri and S. Banerjee, 2018. A flexible discontinuous modulation scheme with hybrid capacitor voltage balancing strategy for three-level NPC traction inverter. *IEEE Transactions on Industrial Electronics*, 66(5) pp.3333-43.

[4] C. Li, T. Yang, P. Kulsangcharoen, G. L. Calzo, S. Bozhko, C. Gerada and P. Wheeler , 2018. A modified neutral point balancing space vector modulation for three-level neutral point clamped converters in high-speed drives. *IEEE Transactions on Industrial Electronics*, 66(2), pp.910-21.

[5] C. Q. Xiang, C. Shu, D. Han, B. K. Mao, X. Wu and T. J. Yu, 2017. Improved virtual space vector modulation for three-level neutral-point-clamped converter with feedback of neutral-point voltage. *IEEE Transactions on Power Electronics*, 33(6), pp.5452-64.

[6] K. K. KS, 2021. Hybrid BIMASGO approach based optimal scheduling of renewable microgrid with multi-period islanding constraints. *International Journal of AdvancedTechnology and Engineering Exploration*, 8(80), p.824.

[7] R. Saravanan, O. Sobhana, M. Lakshmanan and P. Arulkumar, 2023. Fuel cell electric vehicles equipped with energy storage system for energy management: A hybrid JS-RSA approach. *Journal of Energy Storage*, 72, p.108646.

[8] J. M. Guerrero, G. Navarro, C. A. Platero, P. Tian and F. Blázquez, 2020. A novel ground fault detection method for electric vehicle powertrains based on a grounding resistor voltage analysis. *IEEE Transactions on Industry Applications*, 56(5), pp.4934-44.

[9] C. Yong, J. J. Zhang and Z. Y. Chen, 2020. Current observer-based online open-switch fault diagnosis for voltage-source inverter. *ISA transactions*, 99, pp.445-53.

[10] H. Wang, Y. Li, A. Wijesekera, G. J. Kish and Q. Zhao, 2023. Switch open-circuit fault detection and localization for modular multilevel converters based on signal synthesis. *IEEE Journal of Emerging and Selected Topics in Power Electronics*.

[11] Y. Jin, Q. Xiao, H. Jia, Y. Ji, T. Dragičević, R. Teodorescu and F. Blaabjerg, 2022. A novel detection and localization approach of open-circuit switch fault for the grid-connected modular multilevel converter. *IEEE Transactions on Industrial Electronics*. 70(1), pp.112-24.

[12] S.A. Zaki, H. Zhu, J. Yao, A. R. Sayed and M. A. Abdelbaky, 2020. Detection and localization the open and short circuit faults in PV system: A MILP approach. In2020 Asia energy and electrical engineering symposium (AEEES) (pp. 187-193). IEEE.

[13] C. Li, Z. Liu, Y. Zhang, L. Chai and B. Xu, 2019. Diagnosis and location of the open-circuit fault in modular multilevel converters: An improved machine learning method. *Neurocomputing*, 331, pp.58-66.

[14] C. Zhang, H. Wang, Z. Wang and Y. Li, 2023. Active detection fault diagnosis and fault location technology for LVDC distribution networks. *International Journal of ElectricalPower & Energy Systems*, 148, p.108921.

[15] P. Selvakumar and G. Muthukumaran, 2023. An intelligent technique for fault detection and localization of three-level ANPC inverter with NP connection for electric vehicles. *Advances in Engineering Software*, 176, p.103354.

[16] H. Matsumori, T. Kosaka, N. Matsui and S. Saha, 2023. Inverter Power Device Fault Detection and Fail Safe Action Strategy for Electric Vehicle with a Dual Inverter fed Open Winding Motor. *IEEE Transactions on Industry Applications*.

[17] M. Kumar, 2023. Multiple Open Switch Fast Fault Detection and Localization Algorithm for Tolerant CHB-MLI. *IEEE Transactions on Transportation Electrification*.

[18] J. A. Reyes-Malanche and F. J. Villalobos-Pina, E. Cabal-Yepez, R. Alvarez-Salas, C. Rodriguez-Donate, 2021. Open-circuit fault diagnosis in power inverters through currents analysis in time domain. *IEEE Transactions on Instrumentation and Measurement.* 70, pp.1-2.

[19] C. Jiang, H. Liu, P. Wheeler, F. Wu and J. Huo, 2023. An Open-circuit Fault Detection Method of PMSM Fed by Dual Inverter with High Robustness. *IEEE Transactions on Energy Conversion*.

[20] W. Rtibi, L. M'barki, M. Yaich and M. Ayadi, 2021. Implementation of the ACO algorithm in an electrical vehicle system powered by five-level NPC inverter. *Electrical Engineering*, 103, pp.1335-45.

[21] M. W. Ahmad, N. B. Gorla, H. Malik and S. K. Panda, 2020. A fault diagnosis and postfault reconfiguration scheme for interleaved boost converter in PV-based system. *IEEETransactions on Power Electronics*, 36(4), pp.3769-80.

[22] M. Kumar, 2020, Open circuit fault detection and switch identification for LS-PWM H-bridge inverter. *IEEE Transactions on Circuits and Systems II: Express Briefs*, 68(4), 1363-7.

[23] X. Ge, J. Pu, B. Gou and Y. C. Liu, 2017. An open-circuit fault diagnosis approach for single-phase three-level neutral-point-clamped converters. *IEEE Transactions on Power Electronics*, 33(3), pp.2559-70.

[24] S.S. Moosavi, A. Kazemi and H. Akbari, 2019. A comparison of various open-circuit fault detection methods in the IGBT-based DC/AC inverter used in electric vehicle. *Engineering Failure,* 96, pp.223-35.

[25] A. Kersten, K. Oberdieck, A. Bubert, M. Neubert, E. A. Grunditz, T. Thiringer and R. W. De Doncker, 2019. Fault detection and localization for limp home functionality of three-level NPC inverters with connected neutral point for electric vehicles. *IEEETransactions on Transportation Electrification*, 5(2), pp.416-32.

[26] M. Dehghani, Z. Montazeri, O. P. Malik, H. Givi and J. M. Guerrero, 2020. Shell game optimization: A novel game-based algorithm. *International journal of intelligent engineering and systems*, 13(3), pp.246-55.

[27] Q. Q. Li, Z. C. He and E. Li, 2020. The feedback artificial tree (FAT) algorithm. *Soft Computing*, 24, pp. 13413-40.